On the analysis of bonded step lap joints

Rhys Jones[a] DarenPeng[a] John G.Michopoulos[b] NamPhan[c] FilippoBerto[d]

https://doi.org/10.1016/j.tafmec.2017.09.001Get rights and content

Abstract

This paper discusses the stress and strain states in adhesively bonded step lap joints from the perspective of the strain energy density solutions determined via the elastic and elastic-plastic solutions obtained using the computer code A4EI, which as outlined in the US Defence Departments Composite Materials Handbook CMH-17-3G, is the industry standard for designing adhesively bonded joints. Whereas it has previously been shown that the load carrying capacity of an adhesively bonded double lap joint could be estimated using the strain energy density associated with the elastic solution and the critical value of the adhesive strain energy density, the present paper reveals that this approach also yields a reasonable first approximation for the load carrying capacity bonded step lap joints.

Keywords

Bonded step lap joints
Strain energy density
Residual strength
Composite adherend failure

1. Introduction

Bonded step lap joints are used in a number of aircraft, viz: the F-15 horizontal stabilator, the F/A-18 wing, Beech Starship and the Lear Fan [1]. However, whilst the US Defence Departments Composite Materials Handbook CMH-17-3G [1] discusses the design and static strength of bonded joints at length there is little guidance on the growth of disbonds and their effect on operational aircraft. Indeed, the primary recommendation contained in CMH-17-3G is for a no growth design, both for damage in bonded joints and also for delamination and impact damage in composite structures, that is validated via a single full scale fatigue test to two lifetimes. The durability of bonded joints is discussed in Section 10.6 of CMH-17-3G. Here attention is primarily focused on one of the lessons learnt in the PABST program [2], namely how to determine the maximum load bearing capacity of a bonded joint, and on the associated

computer code A4EI [3]. (This code is a continuation of the work reported in [5], [6], [7].) Section 10 of CMH-17-3G also discusses the use of A4EI for the design of bonded repairs to damaged composite structure.

Molski and Glinka [13] were the first to show that in the presence of localised yielding ahead of a notch tip the energy density (W), $W = \int \sigma_{ij} d\varepsilon_{ij}$ where σ_{ij} and ε_{ij} are the stress and strain tensors respectively, calculated using the theoretical elastic stress and strain fielddistribution and that calculated from the stresses and strains determined from an elastic-plastic analysis essentially coincide. (This approximation is sometimes referred to as the Glinka approximation.) This paper first uses the computer code A4EI, which as noted in the industry standard Composite Materials Handbook [1] is routinely used to design and assess bonded joints in composite and adhesively bonded airframes, to illustrate the prior findings presented [14], [15], [16], [17], [18] that for a symmetric double lap joint the maximum value of the strain energy density determined via a purely elastic solution is in good agreement with that calculated using an elasto-plastic analysis. It is then shown that this approximation also holds for adhesively bonded step lap joints.

Refs. [16], [17], [18] concluded that although for adhesively bonded double lap joints the adhesive stresses and strains calculated using A4EI and in the ESDU code [19] are predicated on the assumption that the adhesive is behaving in an elastic perfectly plastic fashion the stresses corresponding to the actual visco-plastic nature of the stress-strain curve can be determined from a knowledge of the strain energy density and the visco-plastic behaviour of the adhesive. This can be achieved by using the fact that the maximum value of the strain energy density in the adhesive is essentially independent both of the nature/shape of the adhesive stress strain curve and also the loading rate. This realisationwhen coupled with the fact that the static strength and durability of the adhesive in adhesively bonded joints and bonded composite repairs is uniquely described by the strain energy density in the adhesive [4], [14], [15], [20] and the fact that, as we will show, the maximum value of the strain energy density in the adhesive determined via a purely elastic solution is in good agreement with that calculated using an elasto-plastic analysis has the potential to simplify both the static strength and fatigue analysis of bonded joints and composite repairs. It also introduces the possibility, as postulated in [21], of using the dissipated energy (in the adhesive) as a criteria for assessing fatigue life of adhesively bonded joints and adhesively bonded repairs to composite airframes in a fashion similar to that outlined in [22], [23] for composite structures.

We also show that whereas A4EI calculates the failure loads associated with failure in the adherends the assumptions used in this estimate are invalid.

2. Background

As explained in [24] Refs. [4], [5], [6], [7] were amongst the first to present closed formanalytical solutions to the problem of adhesively bonded joints, where the adhesive was allowed to deform plasticitly. As noted in [4], [5] these references explained that (1)

> "The adhesive shear strain energy per unit bond area was the necessary and sufficient adhesive characteristic governing the potential bond shear strength." (2)
>
> "The precise shape of the stress-strain curve appeared to be unimportant." This conclusion was supported by independent finite element studies [14], [15], [16], [17], [18], [25].

In this context it should be noted that strain energy density is widely used to assess cracking and the fatigue performance of both metals and composites, see [8], [9], [10], [11], [12]. To further highlight the significance of using as the design parameters the maximum value of the strain energy density energy W ($W = \int \tau \, d\gamma$, where τ and γ are the maximum values of the adhesive shear stresses and shear strain respectively) in the adhesive and W_c, the adhesive critical strain energy density as measured via the ASTM D1002 thick adherend test [26], let us consider a symmetric double lap joint. A schematic representation of the particular symmetric double lap joint to be investigated in this section is shown in Fig. 1. A schematic representation of the elastic-perfectly plastic adhesive shear stress shear strain and the elastic-plastic relationships used in [4] to represent the true adhesive shear stress shear strain relationship of the adhesive is shown in Fig. 2.

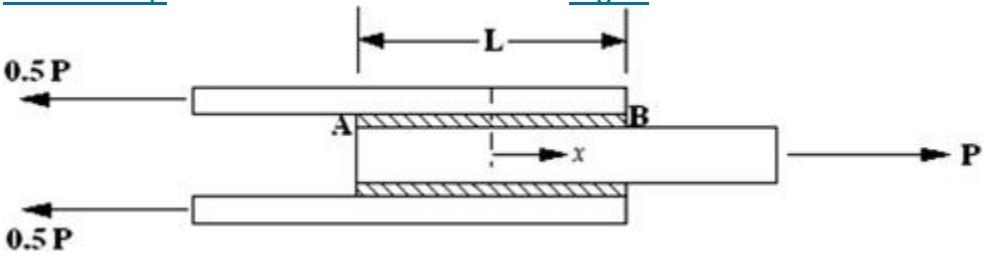

1. Download high-res image (25KB)
2. Download full-size image

Fig. 1. Typical geometry for symmetric double lap joint tests.

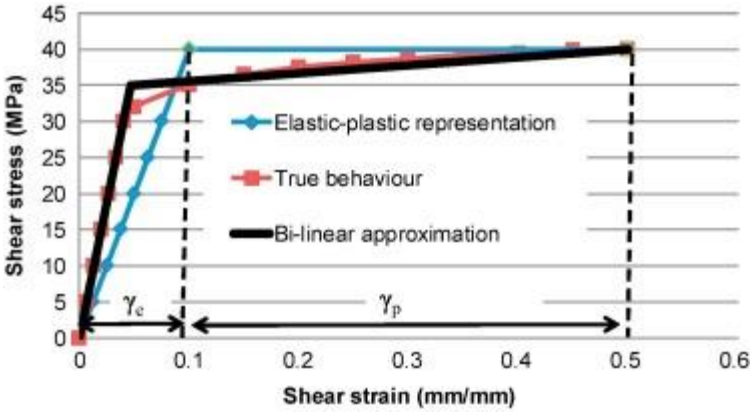

1. Download high-res image (158KB)
2. Download full-size image

Fig. 2. Typical schematic representation of the adhesive shear stress shear strain relationship used in [4].

It is known that the maximum stress in a symmetric double lap joint occurs in the region of the corners 'A' and 'B', see Fig. 1, directly over the joint and at the ends of the lap. It was shown in [14], [15] that for long overlaps and constant adhesive thickness joints under any given load, the strain energy density obtained via a plasticity analysis (W_{EP}), with the adhesive stress strain relationship approximated by the elastic-plastic representation shown in Fig. 2, and that calculated via a purely elastic analysis[1] (W_E), with the elastic shear modulus taken from the elastic-plastic representation shown in Fig. 2, essentially coincide, i.e. that the Glinka approximation holds, viz:

(1)$W_{EP}=W_E$

If the inner and outer adherends are identical and have identical total thicknesses then for long overlap lengths W_{EP} $(= (\tau_{av}l)^2/(4\,Ett_a))$. Here γ_e and γ_p are the elastic and plastic shear strain at A respectively, see Fig. 2, τ_p is the yield stress, E and t are the Young's modulus and the thickness of the adherends respectively and t_a is the adhesive thickness. It is important to note that, as shown in [4], W_{EP} is independent of the elastic (G_e) and post yield (G_p) moduli of the adhesive.

As a result of Eq. (1) the elastic plastic failure load (P_{EP}), i.e. the load estimated using an elastic plastic analysis, can be estimated from a purely elastic analysis. To do this we first need to calculate the adhesive strain energy density (W_E), at the critical point for a load $P_E$which must be such that the corresponding maximum value of the adhesive shear stress is beneath the yield stress of the adhesive. The failure load P_{EP}, associated with the elastic-plastic analysis, can then be estimated using the formulae:

(2)$P_{EP}=P_E\cdot(W_c/W_E)$

where W_c is the adhesive critical strain energy density as measured via the ASTM D1002thick adherend test, see Appendix A.
This finding was confirmed in [14], [15], [16], [17], [18], [25] for both elastic-plastic and visco-plastic adhesives. A discussion on the visco-plastic behaviour of adhesives and the matrix material associated with composite laminates is given in Appendix B The structural response of thin film adhesives and matrix material in composite laminates, Appendix C The structural response of the matrix material in composite laminates respectively. In the next section we will show that running the USAF step lap computer code A4EI confirms that Eq. (2) can also be used to determine an approximate the failure load for adhesively bonded (symmetrical) step lap joints.

3. Application of A4EI to a symmetric double overlap joint

To further illustrate that Eq. (2) can be used to determine the failure loads associated with adhesively bonded double lap joints we used the example given in [3] to validate the computer code A4EI for the USAF. This example consisted of two 0.127 in. (3.23 mm) external aluminium alloy doublers bonded on either side of a 0.254 in. (6.45 mm) thick central aluminium alloy adherend. The Youngs modulus of the aluminium adherends was 68.94 MPa. In [3] solutions are provided for a constant adhesive thickness of 0.005 in. (0.127 mm). In the elastic-plastic analysis presented in [3] the adhesive was assumed to have an elastic perfectly plastic shape with a yield stress τ_p = 5 ksi (34.5 MPa), a shear modulus G_{adh} of 50 ksi (345 MPa) and a maximum strain at failure γ_{max} = 0.5 in./ in. (mm/mm). The resultant predicted failure loads (P_f) obtained using Eq. (2), with the elastic stresses and strains as calculated using A4EI, and the elastic-plastic failure loads determined using A4EI together with an elastic-plastic analysis are shown in Table 1. Analyses were also performed using a 0.01 in. (0.254 mm) thick adhesive and the results are also presented in Table 1. Both solutions coincide with the failure load as determined using the analytical formulae given in [4] for a symmetric double lap joint.

Table 1. Failure loads (lb/in.) for the case G_{adh} = 345 MPa, τ_p = 34.5 MPa, and γ_{max} = 0.5 mm/mm, values in N/mm are in brackets.

	Using Eq. (2)	Using the elastic-plastic strain energy density, from A4EI	% diff
Adhesive thickness = 0.005 in.	10392 (1820)	10392 (1820)	0.0
Adhesive thickness = 0.01 in.	14696 (2573)	14696 (2573)	0.0

The analysis for the case t_a = 0.005 in. (0.127 mm) was then repeated using an adhesive shear modulus G_{adh} = 100 ksi (689 MPa), all other variables being kept the

same, and the resultant predicted failure loads (P_f), as per Eq. (2), are shown in Table 2 together with the failure loads computed using an elastic-plastic analysis. The analysis was then repeated with G_{adh} = 100 ksi (689 MPa), τ_p = 5 ksi (34.5 MPa) and γ_{max} = 0.75 mm/mm and the resultant predicted failure loads are shown in Table 3. In the next example the values used were G_{adh} = 30 ksi (207 MPa), τ_p = 5 ksi (34.5 MPa) and γ_{max} = 0.3 mm/mm. The resultant predicted failure loads are shown in Table 4.

Table 2. Failure loads (lb/in.) for the case G_{adh} = 689 MPa, τ_p = 34.5 MPa, and γ_{max} = 0.5 in./in., values in N/mm are in brackets.

	Using Eq. (2)	Using the elastic-plastic strain energy density, from A4EI	% diff
Adhesive thickness = 0.005 in.	10677 (1870)	10677 (1870)	0.0
Adhesive thickness = 0.01 in.	15100 (2644)	15100 (2644)	0.0

Table 3. Failure loads (lb/in.) for the case G_{adh} = 689 MPa, τ_p = 34.5 MPa, γ_{max} = 0.75 in./in., values in N/mm are in brackets.

	Using Eq. (2)	Using the elastic-plastic strain energy density, from A4EI	% diff
Adhesive thickness = 0.005 in.	13,191 (2310)	13,191 (2310)	0.0

Table 4. Failure loads (lb/in.) for the case G_{adh} = 207 MPa, τ_p = 20.7 MPa and γ_{max} = 0.3, values in N/mm are in brackets.

	Using Eq. (2)	Using the elastic-plastic strain energy density, from A4EI	% diff
Adhesive thickness = 0.005 in.	6000 (1051)	6000 (1051)	0.0

This analysis confirms prior findings that the failure loads predicted using Eq. (2) are in excellent agreement with the analytical values obtained using the formulae given in [4] and the elastic-plastic failure loads computed using A4EI.

4. Analysis of a simple step lap joint

CMH-17-3G [1] explains that much of the methodology currently used in the design and analysis of adhesive step lap joints, see Fig. 3, and scarfed repairs to composite structuresis based on the computer code A4EI [3]. As previously noted this code is an extension of the lap joint analysis developed in [4], [6] and validated as part of the PABST program [2]. As such Eq. (2) should also hold, i.e. the adhesive failure load estimated via the strain energy density computed using the elastic solution and that estimated using the elastic-plastic solution should essentially coincide.

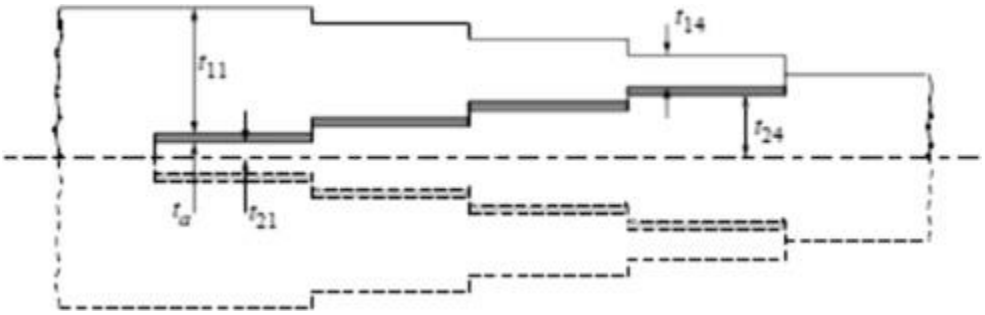

1. Download high-res image (34KB)
2. Download full-size image

Fig. 3. The four step lap joint analysed in [19].

Prior to investigating the use of Eq. (2) to estimate the failure loads for a step lap joint we first analysed the four-step lap joint presented in the ESDU report on bonded lap joints [19]. The geometry of the joint is shown in Fig. 3. The adherends in the ESDU example both had moduli of E = 200,000 MPa, the adhesive had a thickness of 0.1 mm and a strain to failure γ_{max} = 0.5 mm/mm. The step lengths and thicknesses of the adherends are given in Table 5. The stress strain curve used in [19] is shown in Fig. 4. Whilst the adhesive had a failure strain of 0.5 mm/mm [19] only reported the load to a shear strain of 0.1 mm/mm. Thus in the A4EI analysis the Hart-Smith approximation for the adhesive stress strain curve up to a shear strain of 0.1 mm/mm is required. This approximation is also shown in Fig. 4. It corresponds to a G_{adh} = 680 MPa and an adhesive yield stress τ_p = 41 MPa. This approximation gives (approximately) the same area under the shear stress versus shear strain curve. The results of this analysis shown in Table 6 which presents the load required to reach a strain of 0.1 using an elastic-perfectly plastic analysis and also the value calculated using Eq. (2) together with the requirement that the strain energy density at the critical point reaches 2.86 MPa, i.e. the value associated with a strain of 0.1. Here we see that:

(1)

A4EI gave a load that was very close to that quoted in [19].

(2)

The load estimated via Eq. (2) and a fully elastic-plastic analyses were quite similar.

Table 5. Details of the ESDU example.

Step number	t_{1i} (mm)	t_{2i} (mm)	l_i (mm)
i = 1	8.0	1.0	6.0
i = 2	6.0	2.0	6.0

Step number	t_{1i} (mm)	t_{2i} (mm)	l_i (mm)
i = 3	4.0	3.0	6.0
i = 4	2.0	4.0	6.0

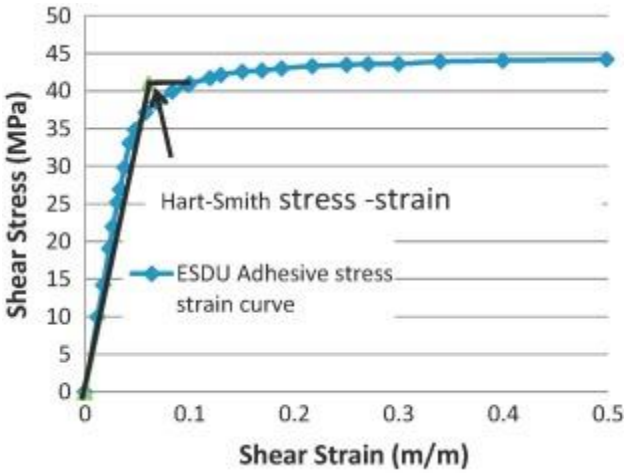

1. Download high-res image (123KB)
2. Download full-size image

Fig. 4. The adhesive stress strain curve used in [19] and the corresponding Hart-Smith approximation.

Table 6. Loads (N/mm) to peak shear strain of 0.1 (mm/mm) for the ESDU four step lap joint, values in (lb/in.) are in brackets.

From [19]	Using Eq. (2)	Using the elastic-plastic strain energy density, from A4EI	% difference between the predicted load using the elastic solution and the value of 1610 N/mm given in [1919]
1610	1689 (9644)	1603 (9153)	4.9

We next used A4EI to analyse the four step joint geometry presented in [33]. The lengths and adherend thicknesses associated with each of the steps is given in Table 7. The adhesive was taken to have a thickness of 0.05 in. (0.127 mm). As in [33] both the inner and outer aluminium adherends were taken to be aluminium with an E = 10^7 psi (68900 MPa).

Table 7. Geometry of the step lap joint, in inches with values in mm in brackets.

i	t_{1i} (in.)	t_{2i} (in.)	l_i (mm) (in.)
1	0.14 (3.556)	0.02 (3.556)	2.0 (50.8)
2	0.12 (3.05)	0.04 (1.016)	0.8 (20.32)
3	0.08 (2.032)	0.08 (2.032)	0.8 (20.32)
4	0.04 (1.016)	0.12 (3.05)	0.8 (20.32)

The following five cases were analysed and the resultant failure loads (P_f) are presented in Table 8.

Case (1) An adhesive yield stress τ_p = 5 ksi (34.5 MPa), an adhesive shear modulus G_{adh} = 50 ksi (345 MPa) and a maximum strain at failure γ_{max} = 0.5 in./ in..

Case (2) An adhesive yield stress τ_p = 5 ksi (34.5 MPa), an adhesive shear modulus G_{adh} = 100 ksi (689 MPa) and a maximum strain at failure γ_{max} = 0.5 in./ in..

Case (3) An adhesive yield stress τ_p = 7.5 ksi (51.7 MPa), an adhesive shear modulus G_{adh} = 50 ksi (345 MPa) and a maximum strain at failure γ_{max} = 0.5 in./ in..

Case (4) An adhesive yield stress τ_p = 3.0 ksi (20.7 MPa), an adhesive shear modulus G_{adh} = 50 ksi (345 MPa)and a maximum strain at failure γ_{max} = 0.5 in./ in..

Case (5) An adhesive yield stress τ_p = 3.0 ksi (20.7 MPa), an adhesive shear modulus G_{adh} = 50 ksi (345 MPa) and a maximum strain at failure γ_{max} = 0.3 in./ in..

Table 8. Failure loads (lb/in.) for the four step lap joint, values in N/mm are in brackets.

	Using Eq. (2)	Using the elastic-plastic strain energy density, from A4EI	% difference
Case 1	14678 (2570)	14645 (2564)	0.2
Case 2	15099 (2644)	15086 (2641)	0.1
Case 3	17468 (3059)	17453 (3056)	0.1
Case 4	11619 (2035)	11531 (2019)	0.8
Case 5	10137 (1775)	10129 (1773)	0.1

To continue this study we examined a 6 step lap joint with the same adherend material properties but with the joint configuration shown in Table 9. The resultant failure loads for the five cases listed are presented in Table 10.

Case (1) An adhesive yield stress τ_p = 5 ksi (34.5 MPa), an adhesive shear modulus G_{adh} = 50 ksi (345 MPa) and a maximum strain at failure γ_{max} = 0.5 in./ in..

Case (2) An adhesive yield stress τ_p = 5 ksi (34.5 MPa), an adhesive shear modulus G_{adh} = 100 ksi (689 MPa) and a maximum strain at failure γ_{max} = 0.5 in./ in..

Case (3) An adhesive yield stress τ_p = 7.5 ksi (51.7 MPa), an adhesive shear modulus G_{adh} = 50 ksi (345 MPa) and a maximum strain at failure γ_{max} = 0.5 in./ in..

Case (4) An adhesive yield stress τ_p = 3.0 ksi (20.7 MPa), an adhesive shear modulus G_{adh} = 50 ksi (345 MPa)and a maximum strain at failure γ_{max} = 0.5 in./ in..
Case (5) An adhesive yield stress τ_p = 3.0 ksi (20.7 MPa), an adhesive shear modulus G_{adh} = 50 ksi (345 MPa) and a maximum strain at failure γ_{max} = 0.3 in./ in..

Table 9. Geometry of the (six) step lap joint, values in mm in brackets.

i	t_{1i} (in.)	t_{2i} (in.)	l_i (in.)
1	0.22 (5.88)	0.04 (5.88)	2.0 (50.8)
2	0.2 (5.88)	0.06 (5.88)	0.8 (20.3)
3	0.16 (5.88)	0.1 (5.88)	0.8 (20.3)
4	0.5 (5.88)	0.14 (5.88)	0.8 (20.3)
5	0.08 (5.88)	0.18 (5.88)	0.8 (20.3)
6	0.04 (5.88)	0.22 (5.88)	0.8 (20.3)

Table 10. Failure loads (lb/in.) for the six step lap joint, values in N/mm are in brackets.

	Using the elastic strain energy density	Using the elastic-plastic strain energy density, from A4EI	% difference (absolute value)
Case 1	25367 (4442)	25306 (4431)	0.2
Case 2	26062 (4564)	26049 (4564)	0.1
Case 3	30197 (5288)	30145 (5279)	0.2
Case 4	20087 (3517)	19982 (3499)	0.5
Case 5	15225 (2666)	15184 (2659)	0.3

In each case we see that for a constant adhesive thickness the failure loads calculated using Eq. (2) and those calculated via the elastic-plastic analyses essentially coincide. Although this paper has focused on step lap joints under axial loading A4EI also has the potential to assess the behaviour under shear loads. Unfortunately it does not allow for a combination of axial and shear loads which is a problem set that is often seen in wing skins. The present paper raises the possibility that since the governing equations for the shear stress induced in the adhesive by shear loading are identical to those for axial loading, albeit with the Young's modulus of the adherends replaced with the shear modulus of the adherends [5], it may be possible to use the strain energy density computed via an elastic analysis of the joint subjected to these combined load states to

generate approximate solutions for the load bearing capacity of a step lap joint subjected to a realistic combination of axial and shear loads.

5. Failure in the composite adherend in a bonded joint

In addition to calculating the load carrying capacity of the adhesive A4EI also estimates if a joint will fail in the composite adherends. However, as mentioned above, whilst it has been established that A4EI yields accurate values for the strain energy density in the adhesive this is not true for its estimate of the stresses in the composite adherends, which are assumed to be a constant through the thickness of the adherends. In reality the large interlaminar stresses developed in composite adherends means that the fibres closest to the joint are stressed the most. To illustrate this tests were performed on a 50 mm wide and 8 mm thick steel double overlap fatigue test specimen where the upper adherends were a 1.2 mm thick unidirectional carbon fibre (CFRP) laminate, see Fig. 5.

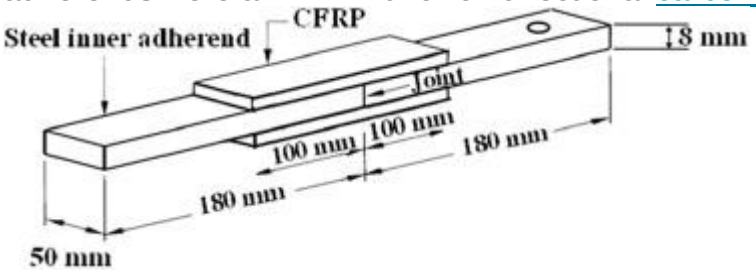

1. Download high-res image (39KB)
2. Download full-size image

Fig. 5. Schematic diagram of the CFRP specimen.

The stress distribution on the surface of the composite adherends was measured using Lock-in infra-red thermography. This approach uses Kelvin's law [31] which states that for a metallic component undergoing cyclic loading at a frequency ω such that the process is essentially adiabatic the changes in temperature ΔT per load cycle are related to changes in the bulk stress $\Delta(\sigma_1 + \sigma_2 + \sigma_3)$

(2)$\Delta(\sigma1+\sigma2+\sigma3)=-\Delta T/(KT0)$

Here T_0 is the absolute base temperature, and K is the thermo-elastic constant. The extension of this formulation to composite structures, including second order effects, is presented in [32]. Thus by extracting the change in temperature that is synchronised with the loading frequency ω we can directly measure the stress field in the structure. The resultant stress field in the vicinity of the joint, see Fig. 5, Fig. 6, is shown in Fig. 7. Here we see a 'camel hump' feature with the surface stresses being maximum on either side of the joint and a minimum stress directly over the joint. The stresses along the line AB in Fig. 7 are shown in Fig. 8 which further highlights the 'camel hump' feature

described above. This finding contrasts with the prediction for the fibre stresses obtained using classical lap jointtheory [4], [6], which are assumed to be constant through the thickness of the adherend and as a result the stresses in the adherend are predicted to be maximum over the joint. As such this finding, which is due to the fact that at the joint the stress in the adherend is not constant through the thickness and that the plies closest to the metal are the most highly stressed [34], invalidates the assumptions inherent in [3], [4], [6] for the stresses in the adherends. This stress gradient results in a local bending moment in the upper adherend which in turn results in the fibre stress on the upper surface being a maximum at a small distance away from the joint. A range of other examples of this “camel hump” feature are given in [35] and a detailed finite element analysis of a typical joint which reveals the complex (non uniform) nature of the stress field through the adherend is given in [34].

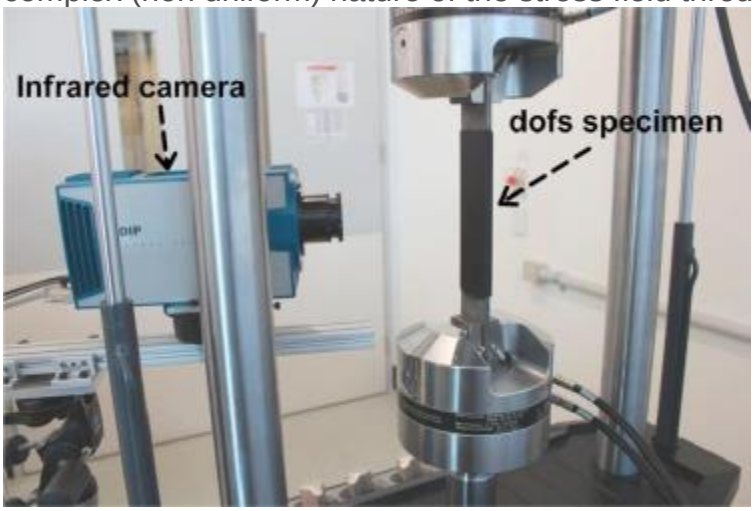

1. Download high-res image (88KB)
2. Download full-size image

Fig. 6. Photograph of the symmetric double overlap fatigue specimen under test.

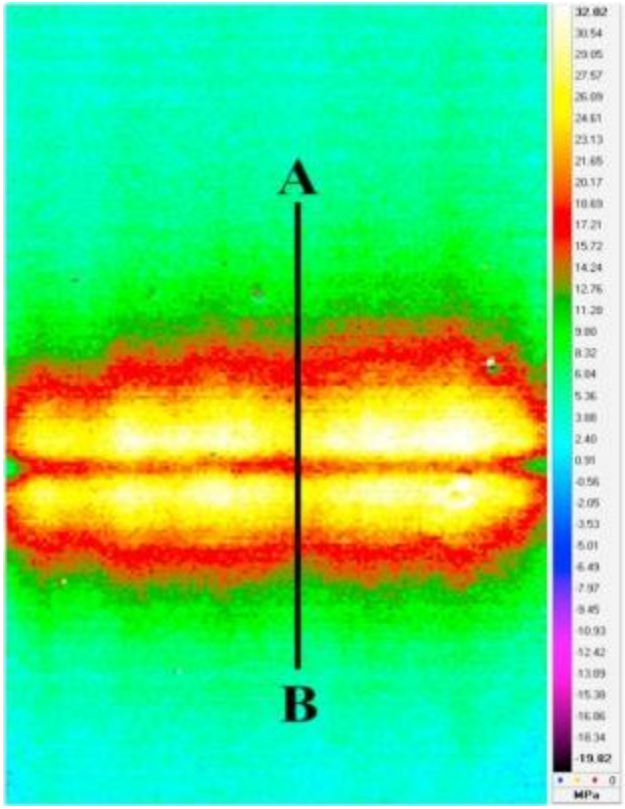

1. Download high-res image (165KB)
2. Download full-size image

Fig. 7. The increment in the stress field on the surface of the patch (upper adherend), from [36].

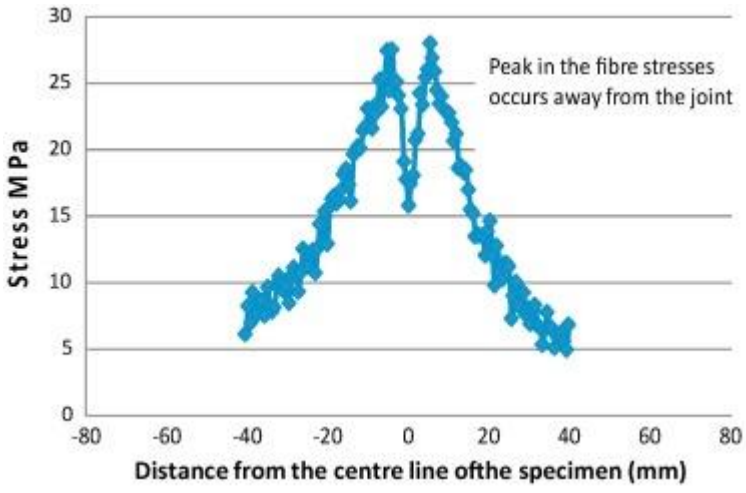

1. Download high-res image (147KB)
2. Download full-size image

Fig. 8. Stresses along line AB in the centre of the patch, from [36].

As previously mentioned the reason for this “camel hump” feature is that, the fibres closest to the joint are the most highly stressed, i.e. they do the most work in restraining the opening of the joint. This finding was first reported in [34], which investigated the stress distribution in a symmetric double lap joint specimen. The specific geometry analysed in [34] was a 6.32 mm thick aluminium inner adherend with a Young’s modulus of E = 73,000 MPa and v = 0.3, whilst the outer adherends were a seven ply thick (0.889 mm) boron epoxy doublerwith E_{11} = 208,000 MPa, $E_{22} = E_{33}$ = 2500 MPa, $v_{13} = v_{23} = v_{12}$ = 0.1677 and $G_{13} = G_{23} = G_{12}$ = 5000 MPa. Here the “1” subscript is in the direction of the load. The outer adherends were assumed to be bonded to the inner aluminium adherend using a 0.13 mm thick adhesive. The adhesive Young’s moduli and Poison’s ratio used in this analysis were E = 1350 MPa and v = 0.35 respectively. The results of this study highlighted the “through-the-thickness” variation in the fibre stresses in the outer composite adhesive directly over the joint, see Table 11 and Fig. 9 which shows the location of the points A and B that are referred to in Table 11.

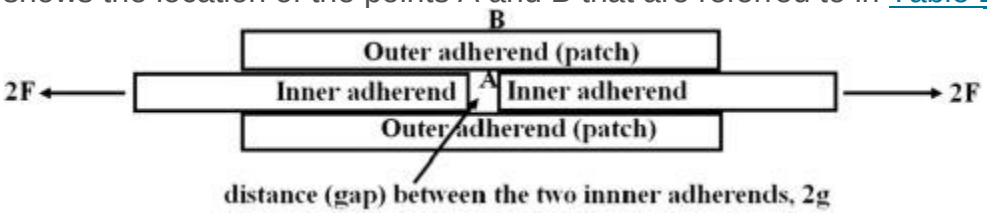

1. Download high-res image (44KB)
2. Download full-size image

Fig. 9. Schematic of the double overlap fatigue specimen analysed [34].

Table 11. Boron Fibre Stresses, from [34]

Gap g (mm)	Fibre stress (σ_f) distribution through Laminate in MPa	
	Point A bottom of the patch, directly over the end of the inner adherend	Point B top of the patch, directly over the end of the inner adherend
8.0	635.0	472.5
4.0	670.0	433.0
2.0	715.0	396.5
1.0	765.0	371.5
0.25	855.0	348.5
0.0	930.0	341.0

On the basis of these results [34] concluded that the approximate theory used in [4], [5], [6]for bonded double lap joints and in A4EI to assess the criticality (residual

strength) of the adherends in a step lap joint is invalid. This conclusion is supported by the experimental data presented above and by the finite element analysis presented in [34]. The importance of allowing for the interlaminar shear stresses that arise in composite adherends is discussed in [34].

This finding, i.e. potentially high interlaminar stresses in the composite adherend over the joint, leads to the question of the residual strength associated with delamination damage that extends from a joint into the composite. In this context it has been shown [33] that for that the problem of delamination damage that extends from a joint into the composite[2] the energy release rate rapidly asymptotes to a constant value so that the residual strength asymptotes to a limiting value as the size of the disbond increases. A similar phenomenon arises for delamination and impact damage in composite structures for which a stage is reached whereby the residual strength essentially remains the same regardless of the size of the damage [38], [39], [40].

It should also be noted that, as explained in [40], in contrast to the situation for cracks in metallic structural components load bi-axiality can have a marked effect on residual strength. This means that for service aircraft the residual strength and the strength after repair cannot be accurately estimated using uni-axial test specimens. As such to tests to evaluate the effect of disbonding, delamination or impact damage on a composite airframe requires the test specimen to be subjected to a three dimensional stress state that reflects (as close as possible) the stress state in the critical region. It should also be noted that as explained in CMH-17-3G the fatigue behaviour of adhesives is strongly load frequency dependent so that tests to assess the effect of disbonds on durability/fatigue life of composite to metal step lap joints should use a representative flight load spectrum with a representative test frequency

6. Conclusion

This paper has shown that using the USAF bonded step lap computer code A4EI confirms the conclusions reached in prior analyses that the load carrying capacity of adhesively bonded double lap joints with a constant adhesive thickness can be estimated from the (purely) elastic solution. We also see that when using A4EI to analyse adhesively bonded multi-step lap joints the failure loads estimated using a purely elastic analysis yields a reasonably good first approximation of those estimated using an elastic-perfectly plastic analysis.

It follows from these findings that whereas the adhesive stresses and strains calculated using A4EI are based on the assumption that the adhesive is behaving in an elastic perfectly plastic fashion, the stresses corresponding to the actual visco-plastic nature of

the adhesive stress-strain curve can be estimated as outlined in [16], [17], [18], as can the energy dissipated during a load cycle. This realisation when coupled with the fact that the static strength and durability of the adhesive is uniquely described by the strain energy density in the adhesive [4] has the potential to simplify the fatigue analysis of such joints, see [18], in a fashion similar to the use of Neuber's hypothesis in the US Navy computer program FAMS [27] for the fatigue assessment of metal structures. It also introduces the possibility of using the dissipated energy (in the adhesive) as a measure of degradation and hence as a criterion for assessing the fatigue life of adhesively bonded joints. This is an important development since dissipated energy is now used to assess the fatigue thresholdsassociated with bonded joints [14], [15], [20].

Whilst this paper has focused on multi-step lap joints under axial loading A4EI also has the potential to assess the behaviour under in-plane shear. However, it does not allow for a combination of axial and in-plane shear which for a wing torsion box is a problem set that is often seen in wing skins. This problem set is particularly important given that disbonds have been detected [37] at the inner wing step lap joint in RAAF F/A-18 aircraft and that at this location the shear loads are approximately 1/3rd of the axial loads. The realisation that the load carrying capacity calculated via a purely elastic and a fully elastic-plastic analysisessentially coincide raises the possibility that since the governing equations for the shear stress induced in the adhesive by shear loading are identical to those for axial loading, albeit with the Young's modulus of the adherends replaced with the shear modulus, it may be possible to generate approximate solutions for the load bearing capacity and the fatigue thresholds of a step lap joint subjected to a realistic combination of axial and shear loads.

We have also seen that whereas A4EI also calculates the failure loads associated with failure in the adherends the assumptions used in this estimate are invalid.

Appendix A. Calculating the failure load from a purely elastic analysis

To calculate the elastic plastic failure load from a purely elastic analysis we first need to calculate the adhesive shear stress, at the critical point, for a load P_E which must be such that the maximum value of the adhesive shear stress is beneath the yield stress of the adhesive. If we denote the corresponding value of the strain energy density, at the critical point, as W_E. Then, in accordance with the Glinka approximation, the failure load P_{EP}, associated with the elastic-plastic analysis, can be estimated using the formulae:

(A1)$$P_{EP}=P_E\cdot(W_c/W_E)$$

Appendix B. The structural response of thin film adhesives and matrix material in composite laminates

As has been discussed in the main text of this paper the stress/strain behaviour of the adhesive and the interlaminar stress strain in the composite play a central role in determining both the load carrying capacity and the fatigue performance of bond joints and composite repairs. The question thus arises: How does a typical structural adhesivebehave?

To answer that question consider the shear stress versus shear strain data presented in [28]for a typical thin film adhesive, viz: FM73, which was determined using a ASTM D 1002 thick adherend test. Fig. 10, Fig. 11 present the shear stress versus shear strain relationships, and the associated predicted responses presented in [28], at a range of strain rates, ~10^{-2}, 10^{-3}, and 10^{-4} per second and temperatures, viz: 23 C (room temperature) and 60 C, see [28]. A more complete description, including the effects of temperature, of the stress strain response of FM73 is given in [28]. Even at room temperature, (i.e. well below its glass transition temperature) there is significant visco-plasticity.

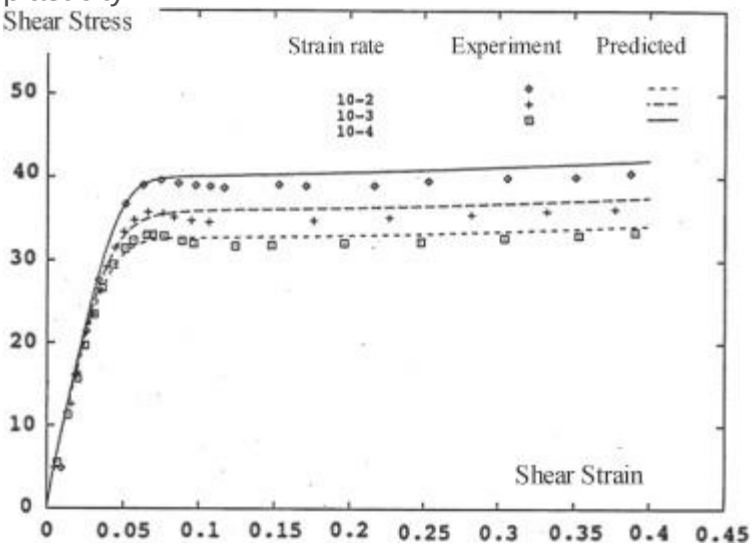

1. Download high-res image (117KB)
2. Download full-size image

Fig. 10. Stress strain curves for FM73 at room temperature, from [28].

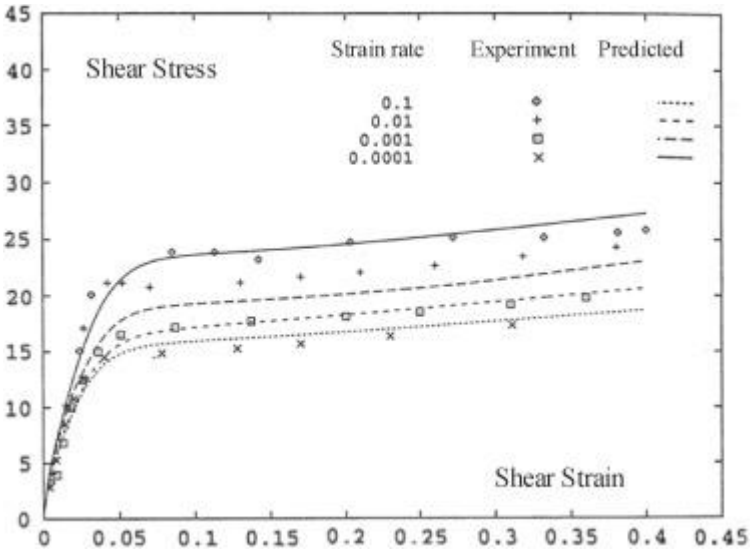

1. Download high-res image (124KB)
2. Download full-size image

Fig. 11. Stress strain curves for FM73 at 60 C, from [28].

Since the yield stress of the adhesive is dependent on the strain rate, it follows that the adhesive properties must have a strong dependence on the loading history. One method of revealing this time dependency, is via a stress-relaxation test (i.e. a strain hold test). Fig. 12shows the result of loading the specimen past yield at a particular strain-rate and then holding the strain at a constant value. This figure reveals a very large stress drop, to a “threshold” value, as a result of the strain hold. The level of the stress relaxation seen in these figures reveals that the “threshold” to which the stress relaxes is independent of the value of the plastic strain, see [28]. The threshold value is also independent of the strain rate and determines the inelastic (irreversible) threshold of the adhesive, i.e. the level beneath which irreversible effects do not occur, and thus the fatigue limit of the adhesive.

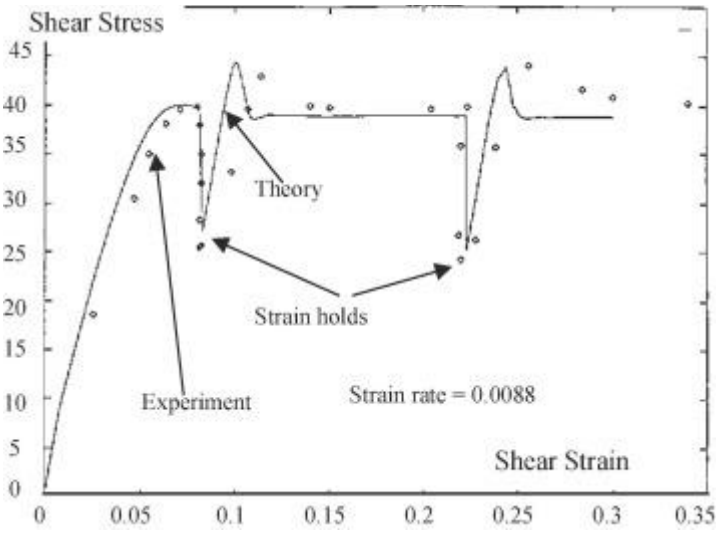

1. Download high-res image (120KB)
2. Download full-size image

Fig. 12. Experimental and predicted response of FM73 during strain holds, from [28].

At this point it should be stressed that, although not mentioned in CMH-17-3G, the requirement that the adhesive stresses should be kept beneath the fatigue limit was a key finding of the USAF PABST program [2] and played a central role in the development of damage tolerant composite repairs to Boeing DC-10 and MD-11 aircraft [29].

Appendix C. The structural response of the matrix material in composite laminates

Having shown how the stress strain behaviour of a typical structural adhesive exhibits significant visco-plasticity let us next examine the non-linear visco-plastic behaviour of composite materials. To determine the matrix dominated shear response tests [30] were performed, using a 100 kN servo-hydraulic INSTRON test machine, in accordance with ASTM standard D3518-76 on a 24 ply $((\pm 45)_{12})_s$ laminate. The specimens were manufactured from a large panel made from AS4/3501 graphite/epoxy. (This material is used in the F/A-18 Classic Hornet and the tests were performed in support of the RAAF F/A-18 fleet.)

The stress/strain behaviour of this graphite/epoxy at various strain rates is shown in Fig. 13, from [30]. These curves again demonstrate the dependencies of the stress/strain behaviour of the composite material on the strain rate. At high shear strain levels the value of shear stress in the material may vary by up to 20% depending on the strain rate applied. For bonded composite joints the local strain field in the composite will vary so

that the local strain rates will vary dependent on its position in the (composite) joint. Therefore, material at a location which sees a high strain will follow a different stress/strain curve to regions away which see a lower strain and therefore a lower strain rate.

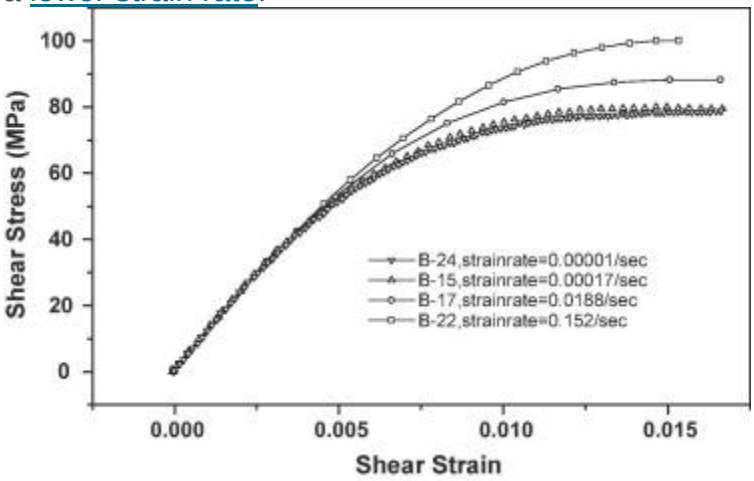

1. Download high-res image (141KB)
2. Download full-size image

Fig. 13. Shear stress/shear strain behaviour of carbon fibre/epoxy resin system AS4/3501-6 at various strain rates, from [30].

The cyclic load results for specimens B-24 and B22 which were tested in [30] at a range of strain rates are shown in Fig. 14, Fig. 15. Fig. 14 shows that the hysteresis curve, for a shear strain rate of 0.00001/s has saturated at about the 5th cycle. Specimens loaded at higher rates require a greater number of cycles to reach saturation, see Fig. 15. Typically for the higher rates, greater than 0.00014/s, about 10 cycles are required before saturation is achieved, see Fig. 15. It is also clear that although there are quite distinct hysterysis loops the (initial) loading and unloading curves appear to be parallel to the initial loading curve.

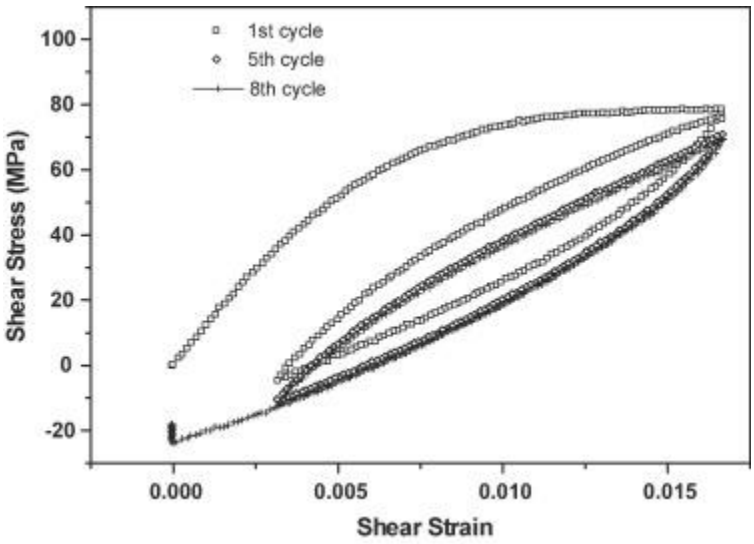

1. Download high-res image (178KB)
2. Download full-size image

Fig. 14. Shear stress/shear strain behaviour of carbon fibre/epoxy resin system AS4/3501-6 under cyclic loading at a strain rate of 0.00001/s (B-24), from [30].

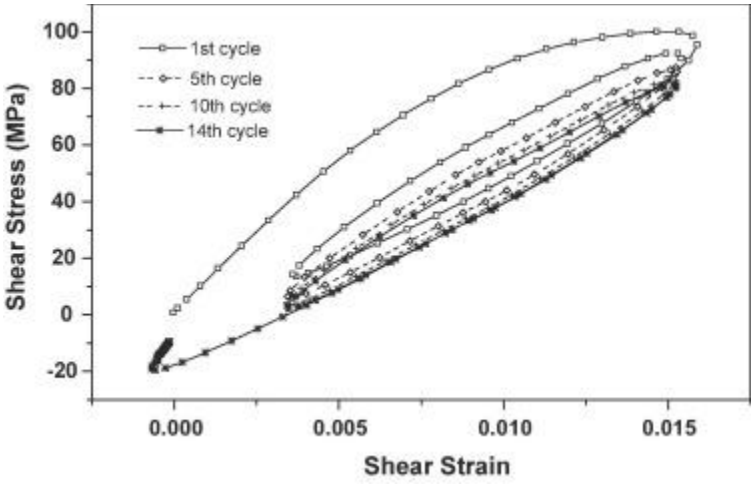

1. Download high-res image (159KB)
2. Download full-size image

Fig. 15. Shear stress/shear strain behaviour of carbon fibre/epoxy resin system AS4/3501-6 under cyclic loading at a strain rate of 0.152/s (B-22), from [30].